



## Improvement in lifetime and replication quality of Si micromold using N:DLC:Ni coatings for microfluidic devices

B. Saha<sup>a</sup>, E. Liu<sup>b</sup>, S.B. Tor<sup>a,b,\*</sup>, D.E. Hardt<sup>a,c</sup>, J.H. Chun<sup>a,c</sup>, N.W. Khun<sup>b</sup>

<sup>a</sup> Singapore-MIT Alliance, Nanyang Technological University, 65 Nanyang Avenue, Singapore 637460, Singapore

<sup>b</sup> School of Mechanical and Aerospace Engineering, Nanyang Technological University, 50 Nanyang Avenue, Singapore 639798, Singapore

<sup>c</sup> Department of Mechanical Engineering, Singapore-MIT Alliance, Massachusetts Institute of Technology, 77 Massachusetts Avenue, Cambridge, USA

### ARTICLE INFO

#### Article history:

Received 30 April 2010

Received in revised form 2 July 2010

Accepted 9 July 2010

Available online 16 July 2010

#### Keywords:

Microfluidic device

Hot embossing

Magnetron co-sputtering

N:DLC:Ni coating

### ABSTRACT

In this paper the effect of surface properties of micromolds on replication process was investigated by using nitrogen (N) and nickel (Ni) doped diamond-like carbon (N:DLC:Ni) coated and uncoated silicon (Si) micromolds. Hot embossing is one of the most popular replication technologies for low cost and mass production. However higher friction and adhesion in hot-embossing process can shorten the lifetime of micromolds. In the micro-hot-embossing process used for this study, the N:DLC:Ni coatings on the Si micromolds successfully increased the lifetime of the micromolds by 3–18 times. The N:DLC:Ni coatings were deposited on the Si micromolds by magnetron co-sputtering at various Ni target powers. The surface and tribological properties of the molds such as bonding structure, surface roughness, surface energy, adhesive strength, friction coefficient and wear resistance were characterized by micro-Raman spectroscopy, atomic force microscopy (AFM), contact angle measurement, micro-scratch test and ball-on-disk sliding test, respectively.

© 2010 Elsevier B.V. All rights reserved.

### 1. Introduction

Diamond-like carbon (DLC) coatings afford an excellent combination of superior tribological and mechanical properties such as low friction and wear and high hardness and modulus of elasticity [1,2], which find their applications in various fields such as cutting and forming tools, heat exchangers, high frequency and high power electronic devices, data storage systems and anti-thrombus coatings [3,4]. However, DLC coatings have some drawbacks such as high residual stress and limitation in thickness, which can be monitored by proper control of deposition parameters [5,6]. It has been reported that metals like Ti, Fe, W, Cr and nonmetals such as Si, N and B, can be used to address the above-mentioned problems of DLC coatings [6–8].

Microfluidic devices are often described as the miniature version of their macro-scale counterparts, and use for biomedical research and clinically useful technologies. The field has considerably grown and branched off into many different areas. Microfluidic devices have many significant advantages such as minimized consumption of reagents, increased automation, reduced manufacturing cost and ability to integrate successive steps in analytical processes on a sin-

gle microfluidic device or multi-level microfluidic device [9–11]. Researchers have started with different materials; among them polymer-based microdevices are indispensable to recent advances in biomedical analysis [10,11]. In particular, these polymer-based microdevices have been applied to many microfluidic platforms owing to their low cost, ease of fabrication, and versatility in preparing complex microstructures [12,13]. Micro-hot-embossing and injection molding processes are the most important replication technologies for microstructures and Si is one of the most popular micromolds in hot embossing and injection molding processes because of its well-established manufacturing processes and good surface finishing [14–16]. A micromold has a large ratio of surface area to volume, which makes it particularly vulnerable to adhesion to molded products or adjacent structures during release [17,18]. Brittleness, relatively high friction and adhesion can cause shorter lifetime of Si micromolds, which discourage to use Si molds.

A few works have been reported on Ni and N doped DLC coatings, which have mainly focused on the bonding configuration of the coatings [19–23]. However, fewer reports have been found on N and Ni codoped DLC-coated micromolds for their tribological properties and replication performance in micromolding polymethyl methacrylate (PMMA) using hot-embossing process. Some researchers also reported fluorinated DLC [24] coatings for molding but thermal stability of this type of coatings is not good [25,26].

In this work, nitrogen and nickel doped N:DLC:Ni coatings were deposited on Si micromolds to enhance the replication performance of the DLC-coated silicon micromolds in hot embossing or

\* Corresponding author at: School of Mechanical and Aerospace Engineering, Nanyang Technological University, 50 Nanyang Avenue, Singapore 639798, Singapore. Tel.: +65 67904725; fax: +65 67922619.

E-mail address: [msbtor@ntu.edu.sg](mailto:msbtor@ntu.edu.sg) (S.B. Tor).

injection molding fabrication processes for microfluidic devices or secondary molds. N and Ni were chosen as doping elements because they could control  $sp^2$  and  $sp^3$  fractions, increase wear resistance and decrease residual stress and friction coefficient of the DLC coatings [7,27]. The N:DLC:Ni coatings were deposited on the Si micromolds via DC magnetron sputtering deposition, during which the sputtering power applied to Ni target was varied to control the structure and properties of the coatings.

## 2. Experiments

### 2.1. DLC coatings on Si micromolds

Before Si micromolds were introduced into the deposition chamber, they were cleaned and degreased by successive rinses in ethanol and deionized water alternatively for eight times and then cleaned in an ultrasonic bath with ethanol for 20 min at 30 °C. Prior to the coating deposition in the deposition chamber, the Ni and C sputter targets and Si substrates were further etched with argon (Ar) plasma using a substrate bias of  $-250$  V for 20 min at an Ar gas pressure of 10 mTorr to remove surface oxide layers.

Ni and N codoped DLC coatings were deposited on Si micromolds by DC magnetron co-sputtering a 4 in. graphite target (99.99% C) and a 4 in. Ni target (99.99% Ni) under a chamber pressure of about 0.4 Pa and a RF (13.56 MHz) bias of  $-100$  V for 30 min. During the DLC depositions, a DC power of 350 W was applied to the C target while different DC powers from 0 to 80 W were applied to the Ni target. Ar and  $N_2$  gases were introduced into the deposition chamber at a fixed flow rate of  $50 \times 10^{-6}$  and  $2 \times 10^{-6}$   $m^3 \text{ min}^{-1}$ , respectively, and the substrates were rotated at 20 rpm during the depositions. The coatings deposited with varying power on the Ni target with an even increment of 20 W were designated as N:DLC, N:DLC:Ni20, N:DLC:Ni40, N:DLC:Ni60 and N:DLC:Ni80.

### 2.2. Characterization

The Raman spectra of the DLC-coated micromolds were recorded from 850 to 2000  $cm^{-1}$  using micro-Raman spectroscopy with a He-Ne ion laser of 633 nm in wavelength to study the bonding configurations of the coatings. Raman parameters such as G peak position and full-width-at-half-maximum (FWHM) and peak intensity ratio ( $I_D/I_G$ ) were determined from the fitted Gaussian peaks. Those parameters were used to signify the  $sp^3$  and  $sp^2$  fractions, cluster size and quality of the coating.

The surface roughnesses of the coated and uncoated Si micromolds were measured by AFM (CSPM-4000) using a  $Si_3N_4$  cantilever in tapping mode with a scan rate of 0.7 Hz for a scan area of  $5 \mu\text{m} \times 5 \mu\text{m}$  inside a closed chamber at an atmospheric condition.

The friction coefficients of the uncoated and DLC-coated Si micromolds were evaluated using a ball-on-disk microtribometer (CMS<sup>TM</sup>) for 3000 laps along a track of 1 mm radius at a sliding speed of  $5 \times 10^{-2}$   $\text{m s}^{-1}$  and a normal load of 1 N at room temperature. PMMA balls of 6 mm in diameter were used as the counterbody to measure the friction forces between the PMMA and micromolds. Scanning electron microscopy (SEM) and surface profilometry were then used to measure the wear scars of the worn surfaces.

The critical loads of the DLC coatings were determined by micro-scratch tester (SST-101, Shimadzu) in a progressive mode with a diamond stylus of 15  $\mu\text{m}$  in radius at a scratching rate of 10  $\mu\text{m s}^{-1}$  for five times. Each sample was measured for five times and SEM micrographs were taken to study the scratch profiles.

A goniometer from Analytical Technologies with a FTA32 software was used to measure contact angles. The contact angles of DI water and ethylene glycol on the different sample surfaces were

**Table 1**

Dispersive ( $\gamma_{lv}^d$ ) and polar ( $\gamma_{lv}^p$ ) components of surface energy of water and ethylene glycol.

Liquid	$\gamma_{lv}^d$ (dyne/cm)	$\gamma_{lv}^p$ (dyne/cm)
DI water	21.8	51
Ethylene glycol	29.3	19

measured for five times and the average values were used to study the wettability of the coatings. The surface energies of the different micromolds were derived from the average contact angles of the two liquids with their known dispersive  $\gamma_{lv}^d$  and polar  $\gamma_{lv}^p$  components as presented in Table 1 [7,18,28].

The glass transition temperature ( $T_g$ ) of the PMMA was determined by differential scanning calorimetry (DSC) using about 10 mg PMMA, which was crimped into an aluminum pan and scanned at a heating rate of 10 °C  $\text{min}^{-1}$ .

A confocal microscope was used to measure the surface profiles of both molds and products with microchannels.

### 2.3. Fabrication of PMMA balls and sheets

The PMMA balls used for the measurement of friction coefficient and the PMMA sheets used as hot-embossing substrates were fabricated by an injection molding process. Melt mass-flow rate, specific gravity and glass transition temperature of PMMA (MH; Teknik Polymers and Colourants) were 0.2 g/min, 1.19 and 115 °C, respectively. The injection temperature and pressure and mold

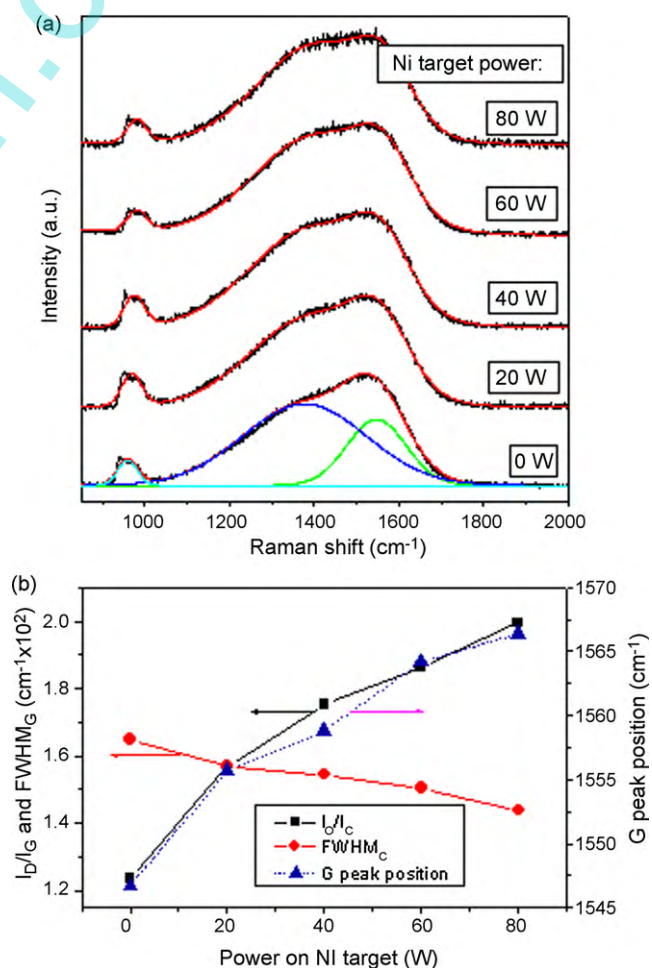


**Fig. 1.** (a) Raman spectra of N:DLC:Ni coatings and (b) G peak position,  $FWHM_G$  and  $I_D/I_G$  with respect to Ni target power.

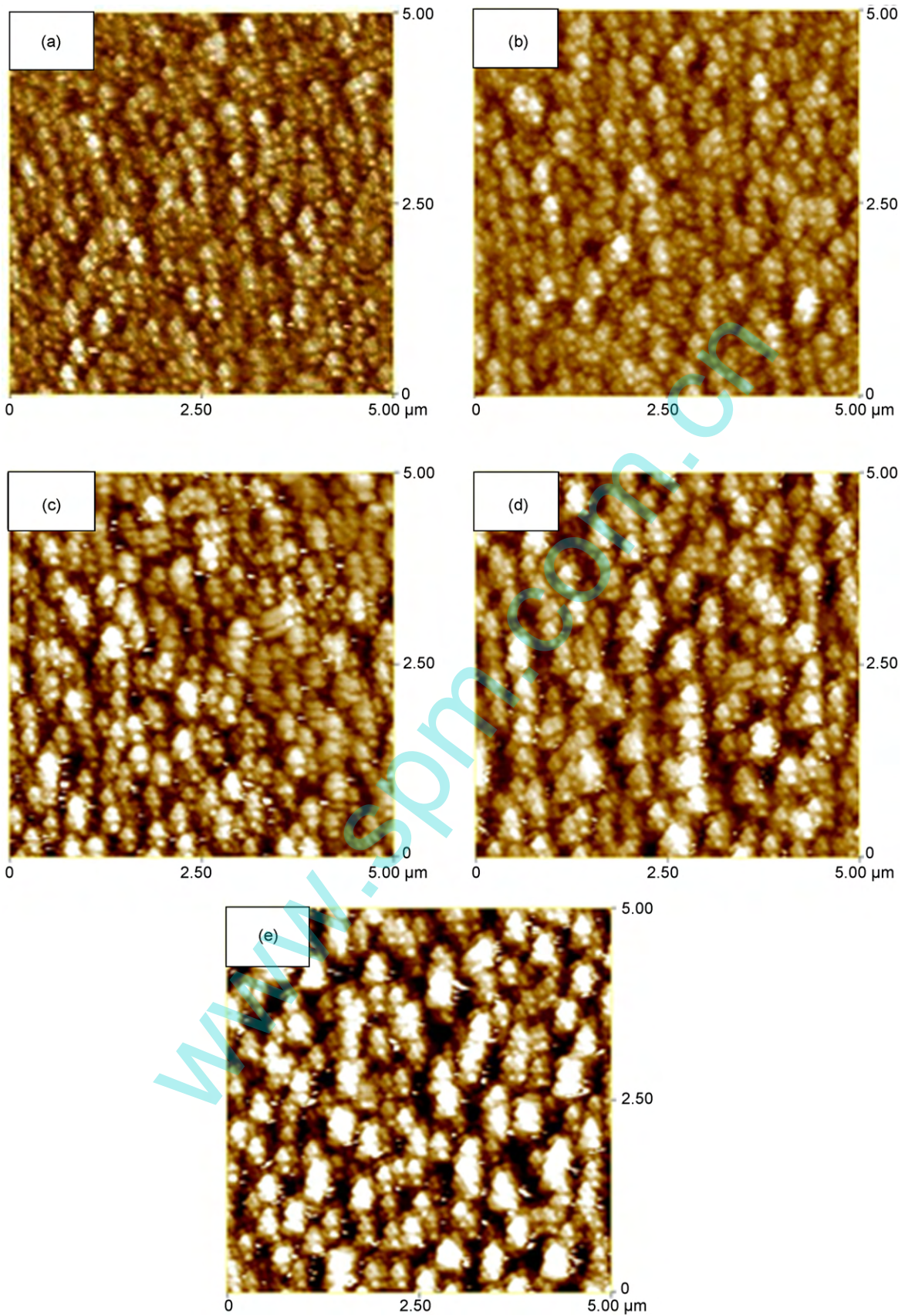


**Fig. 2.** AFM images showing the effect of Ni target power on the surface roughness of N:DLC:Ni coatings: (a) N:DLC, (b) N:DLC:Ni20, (c) N:DLC:Ni40, (d) N:DLC:Ni60 and (e) N:DLC:Ni80.

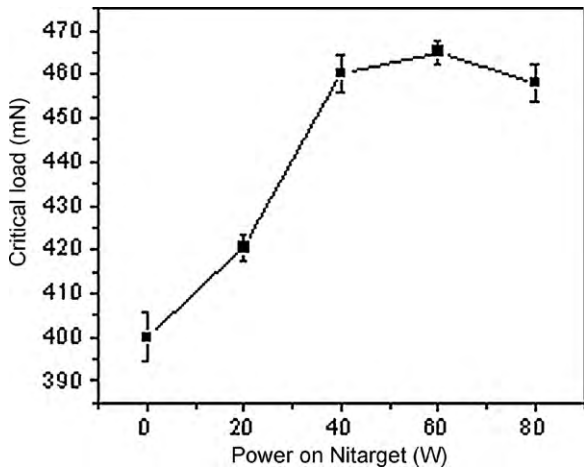


Fig. 3. Critical load of N:DLC:Ni coatings vs. Ni target power.

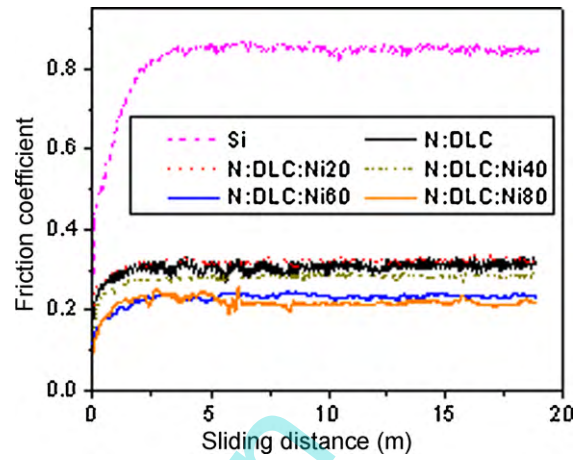


Fig. 4. Friction coefficient vs. sliding distance of N:DLC:Ni coatings tested against PMMA counter ball.

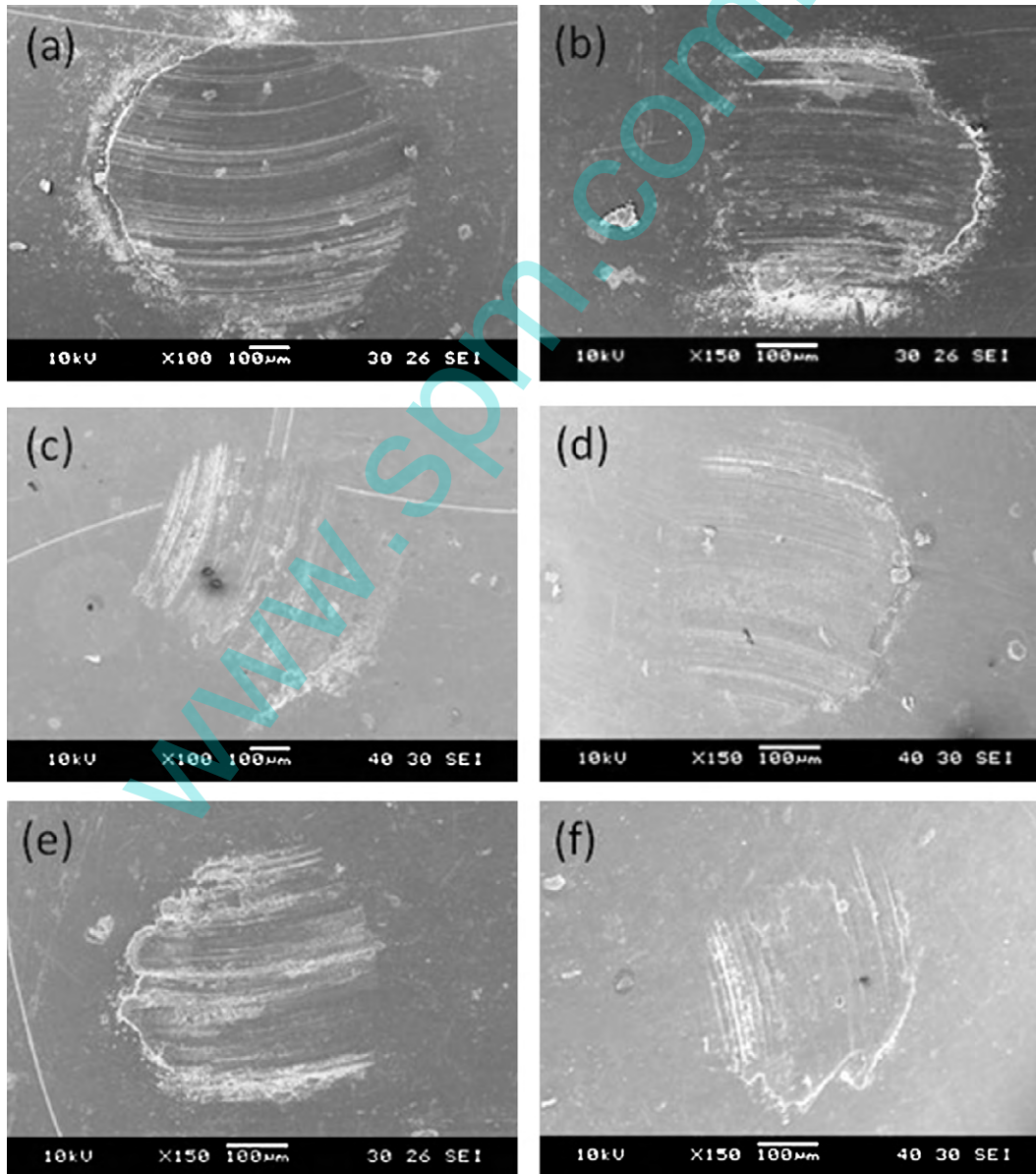


Fig. 5. Wear scar profiles of PMMA balls against (a) bare Si, and (b) N:DLC, (c) N:DLC:Ni20, (d) N:DLC:Ni40, (e) N:DLC:Ni60 and (f) N:DLC:Ni80 coatings.

temperature were about 250 °C, 1100 bar and 60 °C, respectively, for the PMMA sheets and the selected injection and mold temperatures for the balls were about 290 and 80 °C, respectively. The material was pre-dried at about 90 °C for 5 h using a dehumidifying drier before molding.

#### 2.4. Fabrication of microfluidic devices

The replication performances of the uncoated and coated micromolds were studied by a micro-hot-embossing process on the PMMA sheets of 1.5 mm thickness. The Si micromolds used in the hot-embossing process were produced by a deep reactive ion-etching (DRIE) process, which was described elsewhere [7]. A combined profile of temperature, pressure and time based on preliminary experiment and past experience, which has been reported elsewhere [18] was chosen for this study. At first the temperature of the PMMA and Si micromolds was raised to about 120 °C within the time duration of about 150 s. Then the pressure was increased to about 0.44 MPa and held for 120 s. In the end, the system was cooled down to room temperature to about 26 °C, which took about 2400 s.

### 3. Results and discussion

Fig. 1a illustrates the Raman spectra of the samples, which are fitted with two Gaussian peaks at around 1350 and 1550  $\text{cm}^{-1}$  known as D and G peaks, respectively [29]. The G peak position varies from about 1546.7 to 1566.4  $\text{cm}^{-1}$ , caused by the variations in fractions of  $\text{sp}^2$  and  $\text{sp}^3$  bonds in the coatings [30]. A downshift of the G peak position usually indicates an increase in  $\text{sp}^3$  fraction. Fig. 1b shows that the G peak position shifts toward higher positions with increased power on the Ni target, indicating that the fractions of  $\text{sp}^3$  and  $\text{sp}^2$  bonds decrease and increase, respectively, with increased Ni content in the coatings.

The full-width-at-half-maximum (FWHM) of G peak gives information about the cluster size of graphite zone [31]. From Fig. 1b, it is observed that the cluster size of the graphite zone increases with increased Ni content in the coatings, which is in the order of N:DLC < N:DLC:Ni20 < N:DLC:Ni40 < N:DLC:Ni60 < N:DLC:Ni80. The stress of a DLC coating decreases with decrease in  $\text{sp}^3$  content [32], as a higher Ni content in the coating promotes the formation of larger cluster.

A shift of intensity ratio ( $I_D/I_G$ ) of the D and G peaks toward a higher value is observed with an increase in Ni target power, which also indicates a decrease in  $\text{sp}^3$  bonds in the DLC coatings [30]. With increased Ni target power, the Raman spectra lose their symmetry in structure and an asymmetric band indicates a lower percentage of  $\text{sp}^3$  bonds in the DLC coatings [33]. The peaks observed at around 900  $\text{cm}^{-1}$  in all the Raman spectra as shown in Fig. 1a are the second order Si Raman peak.

The surface root-mean-square roughnesses ( $R_q$ ) of the coated Si micromolds are higher than that of the uncoated ones and continuously increase with respect to Ni target power. This can be explained by the FWHM<sub>G</sub> of the Raman spectra. A lower FWHM<sub>G</sub> represents a higher cluster size of graphite zone, which indicates the cause of increase in roughness of the N:DLC:Ni coatings with the increase in the Ni target power. With higher Ni concentrations, a lower dissolution of Ni and a smaller distortion of the DLC matrix could be another reason of increase in surface roughness [27]. The AFM images of the coated and uncoated mold surfaces are shown in Fig. 2, which show the order of the  $R_q$  values in the coatings, i.e. N:DLC (6.3 nm) < N:DLC:Ni20 (8.9 nm) < N:DLC:Ni40 (10.1 nm) < N:DLC:Ni60 (14.6 nm) < N:DLC:Ni80 (16.1 nm).

The adhesion strengths of the coatings with the substrates are determined from the critical loads of the

scratch tests. The critical loads are in the order of N:DLC < N:DLC:Ni20 < N:DLC:Ni40 < N:DLC:Ni60 < N:DLC:Ni80 as shown in Fig. 3. The adhesion strength is influenced by the residual stress in the coatings, which is originated from structural-mismatch, growth-induced stress and/or thermal stress. As the Ni doping leads to a decreased  $\text{sp}^3$  fraction the stress of the N:DLC:Ni coatings decreases with increased Ni target power, which causes the critical load to increase monotonically with respect to Ni target power.

Friction coefficient is one of the dominating characteristics of the demolding process in micro-embossing as the surface-to-volume ratio of a microdevice is very high. Therefore, the friction coefficients of the micromolds have to be minimized through DLC coatings. The friction coefficients between the coated or uncoated micromolds and the PMMA balls with respect to sliding distance are presented in Fig. 4. It is observed that the friction coefficient increases a little with the increase in Ni target power from 0 to 20 W, after which it decreases continuously with further increase in the Ni target power. The increased surface roughness of the coatings in addition to Ni content could be another reason for the increase in friction coefficient. A higher Ni content in the DLC coatings promotes the formation of a large fraction of  $\text{sp}^2$  bonds that act as a solid lubricant [34,35] and cause a continuous decrease in friction coefficient.

The wear scars on the PMMA balls against the micromolds are examined using SEM as shown in Fig. 5, which are in the order of vs. Si (740  $\mu\text{m}$ ) > vs. N:DLC:Ni20 (545  $\mu\text{m}$ ) > vs. N:DLC (456  $\mu\text{m}$ ) > vs. N:DLC:Ni40 (441  $\mu\text{m}$ ) > vs. N:DLC:Ni60 (399  $\mu\text{m}$ ) > vs. N:DLC:Ni80 (322  $\mu\text{m}$ ). This trend is similar to that of friction coefficient and depicts more severe wear of the PMMA material with respect to Ni target power. The wear rate of the PMMA ball is highest when it runs against the bare Si mold because of the highest friction coefficient of this couple. A smallest wear scar is observed from the PMMA ball tested against the N:DLC:Ni80 micromold. The wear of the micromolds is not evident from the measurement by using surface profilometer, which is attributed to the high strength of the micromold materials.

The contact angles of the DLC coated and uncoated Si micromolds were measured using both DI water and ethylene glycol to determine the surface energies of the molds. Fig. 6 shows that the Ni power has a great influence on the contact angles of water and ethylene glycol, which helps identify the optimum Ni target power. The relationship between contact angle and surface energy and its

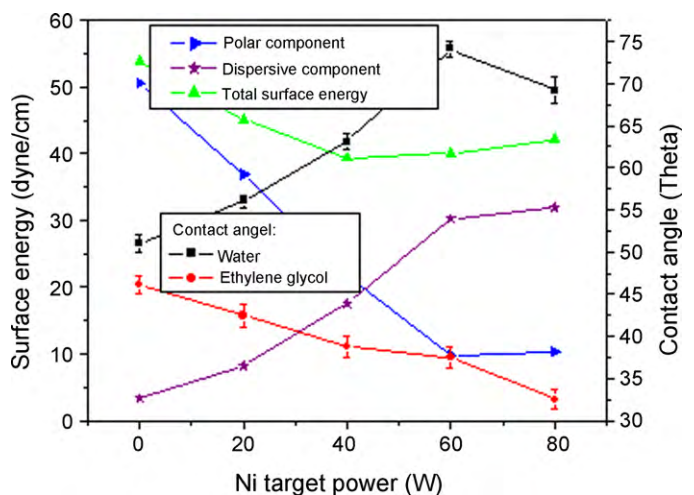
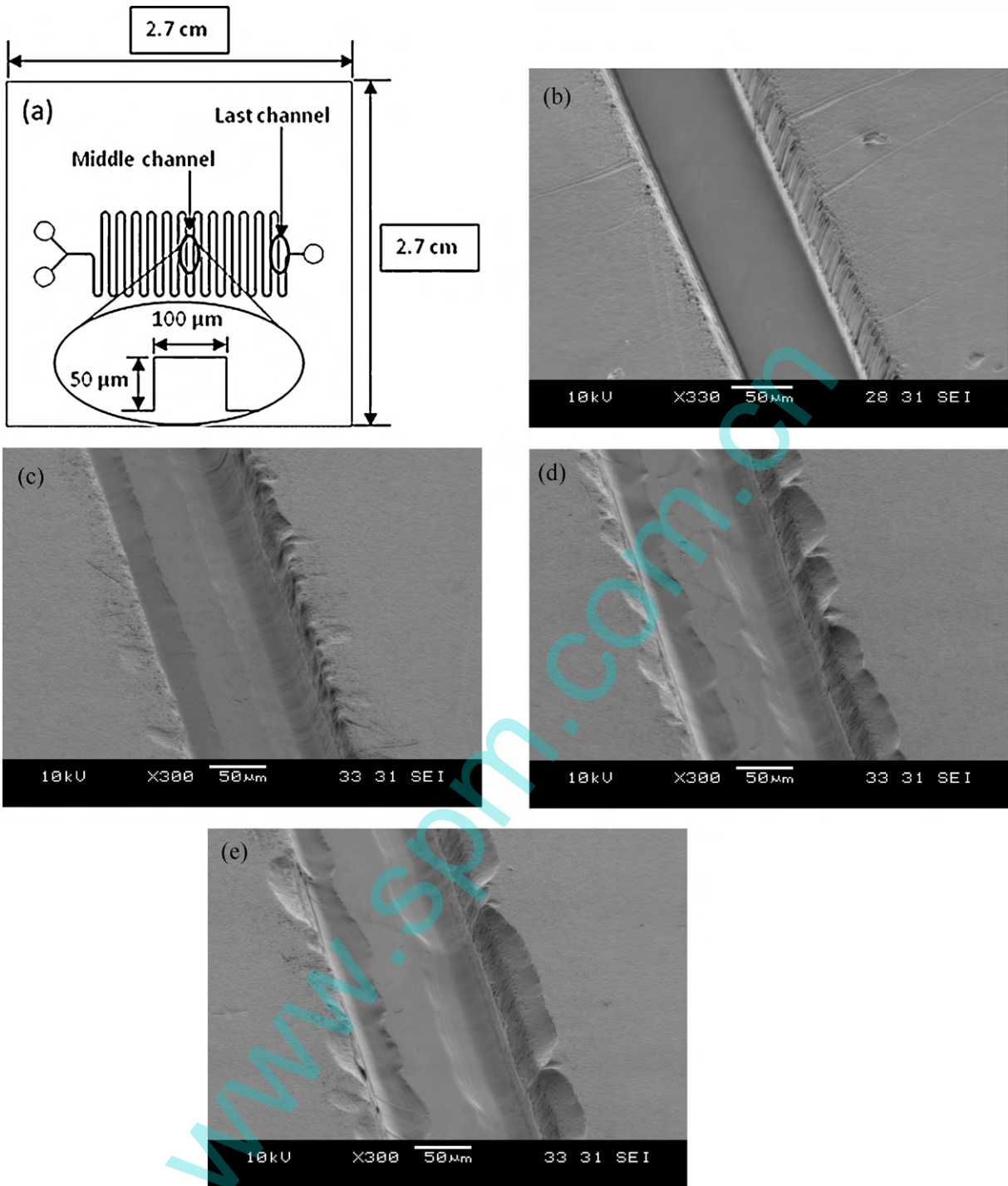


Fig. 6. Measured contact angles of DI water and ethylene glycol and calculated surface energies and their respective dispersive and polar components of N:DLC:Ni coatings with respect to sputtering power on Ni target.



**Fig. 7.** (a) Schematic diagram of Si micromold, (b-c) SEM micrographs of middle channel and last channel of a PMMA microfluidic device fabricated using a coated Si micromold, and (d-e) middle channel and last channel of a PMMA device fabricated using an uncoated Si micromold.

dispersive and polar components are represented by Eqs. (1)–(4) [7,18]

$$\gamma_{sv} = \gamma_{sl} + \gamma_{lv} \cos \theta \quad (1)$$

$$\gamma_{sv} = \gamma_{sv}^d + \gamma_{sv}^p \quad (2)$$

$$\gamma_{lv} = \gamma_{lv}^d + \gamma_{lv}^p \quad (3)$$

$$\gamma_{sl} = \gamma_{sl}^d + \gamma_{sl}^p \quad (4)$$

where  $\gamma$  is the surface energy, superscripts “d” and “p” refer to the dispersive and polar components, respectively, subscripts “sv”, “lv” and “sl” refer to the solid vapor, liquid vapor and solid–liquid interfaces, respectively, and  $\theta$  is the measured contact angle.

The dispersive and polar components of surface energies are related by Eqs. (5) and (6) [13]

$$\gamma_{sl}^d = \gamma_{sv}^d + \gamma_{lv}^d - 2(\gamma_{sv}^d \cdot \gamma_{lv}^d)^{1/2} \quad (5)$$

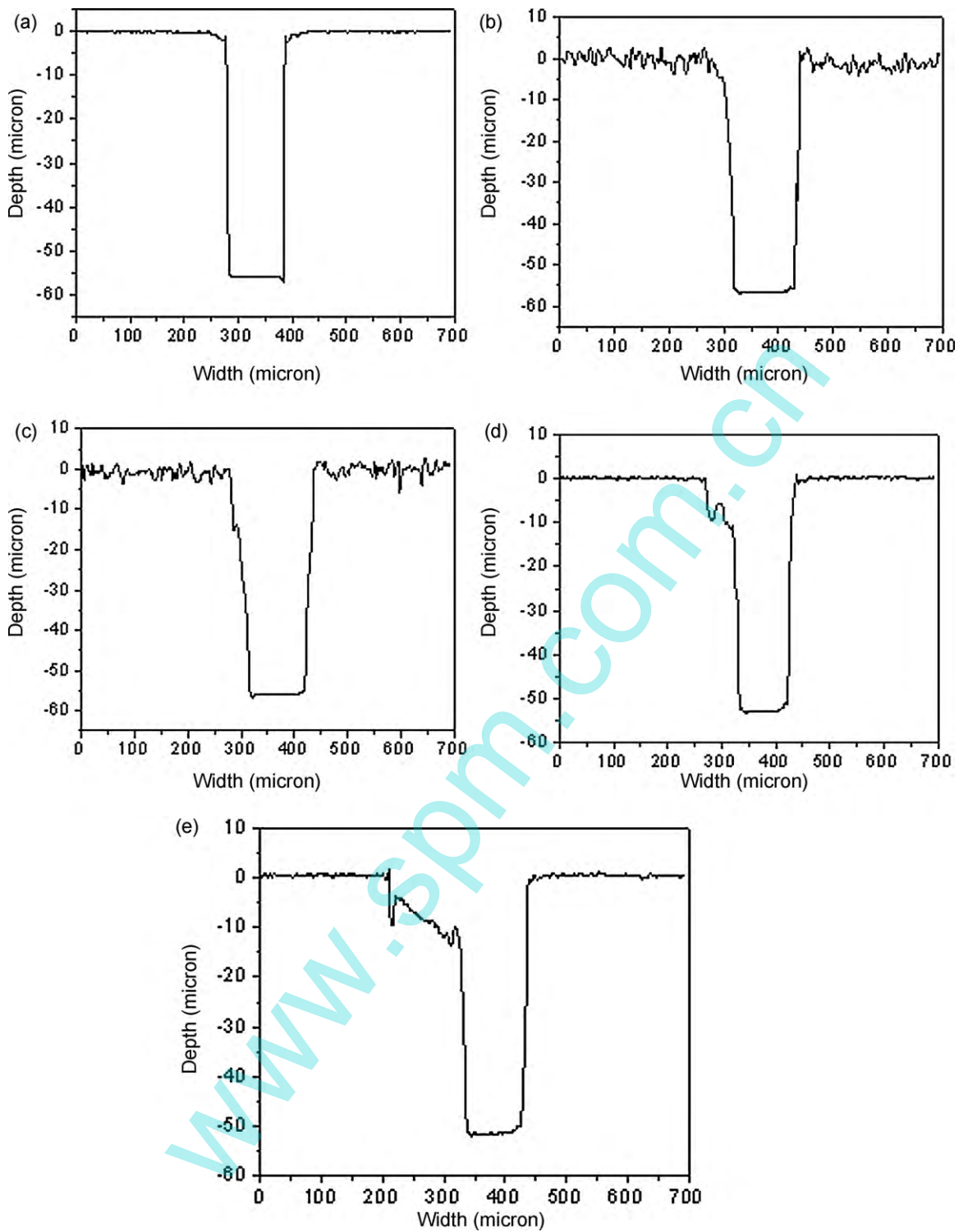


**Fig. 8.** Surface profiles of (a) a channel from a Si micromold, (b) middle channel and (c) last channel of a PMMA microfluidic device using a coated Si micromold, and (d) middle channel and (e) last channel of a PMMA device using an uncoated Si micromold.

$$\gamma_{sl}^p = \gamma_{sv}^p + \gamma_{lv}^p - 2(\gamma_{sv}^p \cdot \gamma_{lv}^p)^{1/2} \quad (6)$$

A correlation is established by combining all above equations, as presented by Eq. (7):

$$(1 + \cos \theta)(\gamma_{lv}^d + \gamma_{lv}^p) = 2(\gamma_{sv}^d \cdot \gamma_{lv}^d)^{1/2} + 2(\gamma_{sv}^p \cdot \gamma_{lv}^p)^{1/2} \quad (7)$$

The dispersive and polar components ( $\gamma_{sv}^d$  and  $\gamma_{sv}^p$ ) of the solid surface energy are calculated by measuring the water and ethy-

lene glycol contact angles ( $\theta$ ) with their known dispersive and polar component ( $\gamma_{lv}^d$  and  $\gamma_{lv}^p$ ) values. It is observed that the surface energy of the N:DLC:Ni coated micromolds decreases with increased Ni target power up to 40 W and then increases slightly with further increased Ni target power. The N:DLC:Ni40 micromold has a good balance between the polar and dispersive components, because of its lowest surface energy among the micromolds. A highest surface energy is observed from the N:DLC micromold, which is followed by the N:DLC:Ni20 one.

The replication performance of the micromoulds is evaluated with respect to number of micro-hot-embossing operations on the PMMA substrates. The friction force decreases and the surface energy also changes for the N:DLC:Ni coated micromolds with respect to Ni target power, which have great effects on the demolding step of the micro-hot-embossing process. A disadvantage of the Si micromolds fabricated by DRIE is that the mold surfaces created during the DRIE process have a high roughness [36]. The friction and adhesion forces increase with increased surface roughness. Therefore, those two factors play a major role in the stresses generated during demolding, which causes the distortions of the microstructures of both the micromolds and the polymeric devices. Based on the experimental results the N:DLC:Ni60 coated micromold was chosen to compare the replication performance with the uncoated Si micromold. A schematic diagram of the Si micromold and the SEM micrographs of the hot embossed tilted microchannels of a PMMA device at two different locations (middle and end channels) are shown in Fig. 7, where it can be seen that the distortions of the microchannels in the both positions using the uncoated micromold are much higher than those from the coated micromold. The reason is because the uncoated micromold has higher friction and adhesion forces than the coated micromold. It is also observed that the distortion of the end channel is higher than that from the middle channel. The side wall contraction force at the edge is high due to a high thermal contraction of PMMA channels, which leads to a higher distortion at the end channel [16]. The uncoated micromolds can be successfully used for about three times in average. The surface profiles of the microchannels at the two above-mentioned positions produced by using both coated and uncoated micromolds are shown in Fig. 8. The PMMA microfluidic device produced using an uncoated micromold in its 3rd operation is shown in Fig. 8d–e that also show higher stretched marks on the side walls of the device due to higher sticking and friction forces. Figs. 7b, c and 8b, c show the SEM micrographs and surface profiles of the PMMA microfluidic devices produced using a coated micromold in its 18th operation. It shows that the replication efficiency of the coated micromolds is much better than that of the uncoated micromolds.

#### 4. Conclusions

Superior N:DLC:Ni coatings were prepared through co-sputtering Ni and graphite targets in a mixed argon–nitrogen deposition environment. Raman spectra confirmed that an increased sputtering power applied to the Ni target increased the  $sp^2$  bonding fraction in the DLC matrix as revealed by a G peak shift from about 1546.7 to 1566.4  $cm^{-1}$ . The surface roughness of the coated micromolds was higher than the uncoated ones and a maximum roughness ( $R_q$ ) of 16.1 nm was observed from N:DLC:Ni80 coated surface. The critical load of the coated micromolds increased with the addition of Ni in the coatings and the N:DLC:Ni60 mold showed a highest critical load of about 465 mN. A lowest friction coefficient of about 0.22 was measured with the N:DLC:Ni80 micromold against a PMMA ball and a smallest wear scare of about 322  $\mu m$  was observed on the PMMA ball surface. The surface energy of the coated micromolds first decreased with increased Ni target power till 40 W and then increased with further increased Ni target power. The N:DLC:Ni40 micromold showed a lowest surface energy of about 39.3 dyne/cm.

The friction force caused by the surface adhesion and the difference in thermal shrinkages of the micromold and PMMA was the main source of the demolding force. The N:DLC:Ni coatings reduced the surface adhesion and friction coefficient, leading to better quality and longer lifetime of the coated micromolds by bet-

ter replication and extended lifetime of the Si micromolds from about 3–18 times in the hot-embossing process.

#### Acknowledgements

This work was supported by the Singapore MIT Alliance (SMA), Nanyang Technological University, Singapore and Massachusetts Institute of Technology (MIT), USA.

#### References

- [1] W. Tillmann, E. Vogli, F. Hoffmann, Wear-resistant and low-friction diamond-like-carbon (DLC)-layers for industrial tribological applications under humid conditions, *Surf. Coat. Technol.* 204 (2009) 1040–1045.
- [2] A.A. Voevodin, C. Rebbholz, A. Matthews, Comparative tribology studies of hard ceramic and composite metal-DLC coatings in sliding friction conditions, *Tribol. Trans.* 38 (1995) 829–836.
- [3] M. Najam-ul-Haq, M. Rainer, C.W. Huck, P. Hausberger, H. Kraushaar, G.K. Bonn, Nanostructured diamond-like carbon on digital versatile disc as a matrix-free target for laser desorption/ionization mass spectrometry, *Anal. Chem.* 80 (2008) 7467–7472.
- [4] H. Fukui, J. Okida, N. Omori, H. Moriguchi, K. Tsuda, Cutting performance of DLC coated tools in dry machining aluminum alloys, *Surf. Coat. Technol.* 187 (2004) 70–76.
- [5] D. Batory, T. Blaszczyk, M. Clapa, S. Mitura, Investigation of anti-corrosion properties of Ti:C gradient layers manufactured in hybrid deposition system, *J. Mater. Sci.* 43 (2008) 3385–3391.
- [6] C.Y. Nie, A. Ando, C.C. Lu, B. Liao, Effect of Ti-doping and stress relaxation layer on adhesion strength of DLC thin film, *Gongneng Cailiao/J. Funct. Mater.* 40 (2009) 226–229.
- [7] B. Saha, E. Liu, S.B. Tor, N.W. Khun, D.E. Hardt, J.H. Chun, Anti-sticking behavior of DLC-coated silicon micro-molds, *J. Micromech. Microeng.* 19 (2009) 105025.
- [8] M. Ban, T. Hasegawa, Internal stress reduction by incorporation of silicon in diamond-like carbon films, *Surf. Coat. Technol.* 162 (2003) 1–5.
- [9] L. Malic, D. Brassard, T. Veres, M. Tabrizian, Integration and detection of biochemical assays in digital microfluidic LOC devices, *Lab Chip* 10 (2010) 418–431.
- [10] M. Mir, A. Homs, J. Samitier, Integrated electrochemical DNA biosensors for lab-on-a-chip devices, *Electrophoresis* 30 (2009) 3386–3397.
- [11] W. Zhang, S. Lin, C. Wang, J. Hu, C. Li, Z. Zhuang, Y. Zhou, R.A. Mathies, C.J. Yang, PMMA/PDMS valves and pumps for disposable microfluidics, *Lab Chip* 9 (2009) 3088–3094.
- [12] P.P. Shiu, G.K. Knopf, M. Ostojic, S. Nikumb, Rapid fabrication of tooling for microfluidic devices via laser micromachining and hot embossing, *J. Micromech. Microeng.* 18 (2008) 025012.
- [13] A. Bendada, A. Derdouri, M. Lamontagne, Y. Simard, Analysis of thermal contact resistance between polymer and mold in injection molding, *Appl. Therm. Eng.* 24 (2004) 2029–2040.
- [14] G. Fu, S. Tor, N. Loh, B. Tay, D.E. Hardt, A micro powder injection molding apparatus for high aspect ratio metal micro-structure production, *J. Micromech. Microeng.* 17 (2007) 1803–1809.
- [15] G. Fu, S.B. Tor, N.H. Loh, D.E. Hardt, Micro-hot-embossing of 316L stainless steel micro-structures, *Appl. Phys. A: Mater. Sci. Process.* 97 (2009) 925–931.
- [16] G. Fu, S.B. Tor, N.H. Loh, B.Y. Tay, D.E. Hardt, The demolding of powder injection molded micro-structures: analysis, simulation and experiment, *J. Micromech. Microeng.* 18 (2008) 075024.
- [17] C.H. Hsueh, S. Lee, H.Y. Lin, L.S. Chen, W.H. Wang, Analyses of mechanical failure in nanoimprint processes, *Mater. Sci. Eng. A* 433 (2006) 316–322.
- [18] B. Saha, E. Liu, S.B. Tor, N.W. Khun, D.E. Hardt, J.H. Chun, Replication performance of Si–N–DLC-coated Si micro-molds in micro-hot-embossing, *J. Micromech. Microeng.* 20 (2010) 045007.
- [19] N. Benchikh, F. Garrelie, C. Donnet, B. Bouchet-Fabre, K. Wolski, F. Rogemond, A.S. Loir, J.L. Subtil, Nickel-incorporated amorphous carbon film deposited by femtosecond pulsed laser ablation, *Thin Solid Films* 482 (2005) 287–292.
- [20] G.J. Kovacs, I. Bertoti, G. Radnoczi, X-ray photoelectron spectroscopic study of magnetron sputtered carbon-nickel composite film, *Thin Solid Films* 516 (2008) 7942–7946.
- [21] T. Ujvari, A. Toth, G.J. Kovacs, G. Safran, O. Geszti, G. Radnoczi, I. Bertoti, Composition, structure and mechanical property analysis of DC sputtered C-Ni and CNx-Ni nano-composite layers, *Surf. Interface Anal.* 36 (2004) 760–764.
- [22] G. Abrasonis, G.J. Kovacs, L. Ryves, M. Krause, A. Mucklich, F. Munnik, T.W.H. Oates, M.M.M. Bilek, W. Moller, Phase separation in carbon-nickel films during hyperthermal ion deposition, *J. Appl. Phys.* 105 (2009) 083518.
- [23] G.J. Kovacs, A. Koos, G. Bertoni, G. Safran, O. Geszti, V. Serin, C. Colliex, G. Radnoczi, Structure and spectroscopic properties of C-Ni and CNx-Ni nanocomposite films, *J. Appl. Phys.* 98 (2005) 034313.
- [24] K. Nakamatsu, N. Yamada, K. Kanda, Y. Haruyama, S. Matsui, Fluorinated diamond-like carbon coating as antisticking layer on nanoimprint mold, *Jpn. J. Appl. Phys.* 45 (2006) L954–L956.
- [25] X. Liu, X. Zhou, J. Gao, Influence of nitrogen doping on thermal stability of fluorinated amorphous carbon thin films, *Trans. Nonferrous Met. Soc. China* 16 (2006) 54–58.

- [26] L. Valentini, E. Braca, J.M. Kenny, G. Fedosenko, J. Engemann, L. Lozzi, S. Santucci, Nitrogen doping of fluorinated amorphous carbon thin films: structural and optical properties evolution upon thermal annealing, *Thin Solid Films* 408 (2002) 291–296.
- [27] G. Yang, E. Liu, N.W. Khun, S.P. Jiang, Direct electrochemical response of glucose at nickel-doped diamond like carbon thin film electrodes, *J. Electroanal. Chem.* 627 (2009) 51–57.
- [28] D.H. Kaelble, J. Moacanin, Surface-energy analysis of bioadhesion, *Polymer* 18 (1977) 475–482.
- [29] R.L. Li, J.P. Tu, C.F. Hong, D.G. Liu, D.H. Zhou, H.L. Sun, Microstructure and tribological properties of Ti-contained amorphous carbon film deposited by DC magnetron sputtering, *J. Appl. Phys.* 106 (2009) 123508.
- [30] N.W. Khun, E. Liu, G.C. Yang, W.G. Ma, S.P. Jiang, Structure and corrosion behavior of platinum/ruthenium/nitrogen doped diamondlike carbon thin films, *J. Appl. Phys.* 106 (2009) 013506.
- [31] M. Kahn, M. Cekada, T. Schoberl, R. Berghauser, C. Mitterer, C. Bauer, W. Waldhauser, E. Brandstatter, Structural and mechanical properties of diamond-like carbon films deposited by an anode layer source, *Thin Solid Films* 517 (2009) 6502–6507.
- [32] S. Xu, D. Flynn, B.K. Tay, S. Praver, K.W. Nugent, S.R.P. Silva, Y. Lifshitz, W.I. Milne, Mechanical properties and Raman spectra of tetrahedral amorphous carbon films with high sp<sup>3</sup> fraction deposited using a filtered cathodic arc, *Phil. Mag. B* 76 (1997) 351–361.
- [33] P. Papakonstantinou, P. Lemoine, Influence of nitrogen on the structure and nanomechanical properties of pulsed laser deposited tetrahedral amorphous carbon, *J. Phys. Condens. Matter* 13 (2001) 2971–2987.
- [34] E. Dekempeneer, K. Van Acker, K. Vercammen, J. Meneve, D. Neerincx, S. Eufinger, W. Pappaert, M. Sercu, J. Smeets, Abrasion resistant low friction diamond-like multilayers, *Surf. Coat. Technol.* 142 (2001) 669–673.
- [35] J. Robertson, Diamond-like amorphous carbon, *Mater. Sci. Eng. R* 37 (2002) 129–281.
- [36] D.L. Henann, L. Anand, Microscale thermoplastic forming of bulk metallic glasses: numerical simulations and experiments, in: *5th International Symposium on Nanomanufacturing*, vol. 40, 2008.

## Biographies

**Biswajit Saha** is pursuing his PhD degree in Singapore MIT Alliance, Nanyang Technological University, Singapore. His PhD work focuses on the micromolding, microfluidic device and tribology.

**Dr. Erjia Liu** is the Director of the Tribology Laboratory and an associate professor with the School of Mechanical and Aerospace, Nanyang Technological University, Singapore. His research includes thin films and coatings, carbon materials, and nanomaterials for tribology, electrochemistry and microfabrication.

**Dr. Shu Beng Tor** obtained his PhD from University of Westminster (formerly Polytechnic of Central London) in 1986. He is the Associate Chair (academic) of the School of Mechanical & Aerospace Engineering, NTU. He was the head of Division of Manufacturing Engineering, Chairman of Strategic Research Area on Engineering Design & Modelling. He was also the Director of the Design Research Centre and Director of Strategic Research Program: Product Design and Realisation. He is a Singapore MIT Alliance (SMA) fellow. Tor's research focuses on Micro-replication processes, Tooling for micro-replication, Mold and tooling Design and Process Threads Automation.

**Dr. David E. Hardt** is a Professor of Mechanical Engineering at the Massachusetts Institute of Technology, USA. His research includes process design and process control for micro-fabrication of polymers, including hot micro-embossing and micro-contacting printing.

**Dr. Jung Hoon Chun** is the Director of the Laboratory for Manufacturing and Productivity and a professor of mechanical engineering at the Massachusetts Institute of Technology, USA. His field of research is the development of innovative manufacturing processes widely used in the electronics, semiconductor, pharmaceutical and renewable energy devices industries.

**Nay Win Khun** is currently a candidate for PhD degree with the School of Mechanical and Aerospace Engineering, Nanyang Technological University, Singapore. His PhD research focuses on nanocomposite diamond-like carbon thin films.